Detailed X-ray Spectral Modeling of ~~Cir X-1~~ CAL87 based on Radiative Transfer

Tsujimoto et al. (2024), ApJ, 960, 46
Tominaga et al. (2023), ApJ, 958, 52
Tominaga (2024), Ph.D. thesis, UoT

M. Tsujimoto[1], M. Tominaga[1,2]

[1]JAXA ISAS, [2]U. of Tokyo,

ブラックホール大研究会@御殿場 (2024/03/01)

いいたいこと

- XRISM があがったのはいいけれど、、、
- スペクトルを活かすには、X 線で使える一般的な RT コードが必要
- 私見では、既存のコードは観測データの質に到底マッチしていない
- X 線分光で使える一般的な RT コードを開発しましょう

Outline

Outline

X-ray line spectroscopy with XRISM

- X-ray line spectroscopy of X-ray binaries & AGNs with XRISM.
- Lines (intensity, shift, profile) probe local $\vec{v}$, n, T structures.

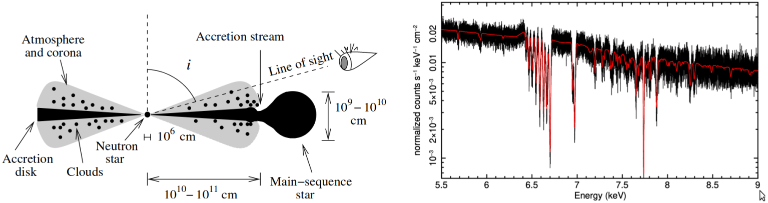

Figure 1. (left) Concept of LMXB structure (Jimenez-Garate+02). (right) Simulated XRISM spectrum of GRS1915+105 (XRISM quick ref guide)

- Strong radiation field from BH/NS/WD governs:
  - Charge & level populations n_i^c (NLTE).
  - Thermal structure T (radiative cooling/heating).
  - Dynamical structure $\vec{v}$ (radiation driven winds).

X-ray line spectroscopy with XRISM

- X-ray line spectroscopy of X-ray binaries & AGNs with XRISM.
- Lines (intensity, shift, profile) probe local $\vec{v}$, n, T structures.

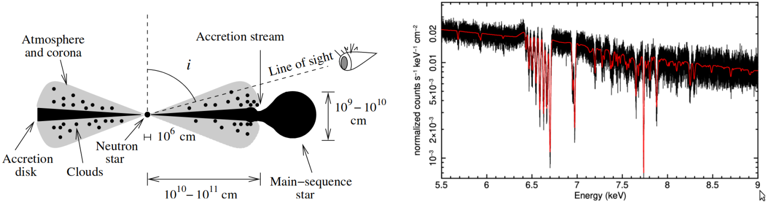

Figure 1. (left) Concept of LMXB structure (Jimenez-Garate+02). (right) Simulated XRISM spectrum of GRS1915+105 (XRISM quick ref guide)

- Strong radiation field from BH/NS/WD governs:
  - Charge & level populations n_i^c (NLTE).
  - Thermal structure T (radiative cooling/heating).
  - Dynamical structure $\vec{v}$ (radiation driven winds).

Optical thickness τ_ν

τ_ν changes drastically as ν.
Assume a typical photoionized plasma around AGNs and X-ray binaries.

- $N_\mathrm{H} = 10^{24}$ cm^{-2}.
- $\log \xi = 3$, where ionization par $\xi = \frac{L_X}{4\pi n_e r^2}$

↓

- For continuum (electron scattering), $\tau_\mathrm{es} = N_\mathrm{H}\sigma_\mathrm{Th} = 0.67$
- For line (e.g., Fe XXV Heα resonance), $\tau_{\mathrm{Fe\ He}\alpha,r} = 4.7 \times 10^3$

$$\tau_{\mathrm{Fe\ He}\alpha,r} = \frac{1}{4\pi\epsilon_0}\frac{\pi e^2}{m_\mathrm{e}c} g f \frac{1}{\sqrt{\pi}\Delta\nu_\mathrm{D}} N_\mathrm{H} A_\mathrm{Fe} A_{24+} A_{1s},$$

$$\Delta\nu_\mathrm{D} \equiv \frac{E_0}{hc}\sqrt{\frac{2k_\mathrm{B}T}{m_\mathrm{Fe}}}$$

- Medium can be $\tau < 1$ for continuum & $\tau \gg 1$ for lines.

Optical thickness τ_ν

τ_ν changes drastically as ν.
Assume a typical photoionized plasma around AGNs and X-ray binaries.

- $N_{\rm H} = 10^{24}$ cm^{-2}.
- $\log \xi = 3$, where ionization par $\xi = \frac{L_X}{4\pi n_e r^2}$

$$\downarrow$$

- For continuum (electron scattering), $\tau_{\rm es} = N_{\rm H}\sigma_{\rm Th} = 0.67$
- For line (e.g., Fe XXV Heα resonance), $\tau_{\rm Fe\ He\alpha,r} = 4.7 \times 10^3$

$$\tau_{\rm Fe\ He\alpha,r} = \frac{1}{4\pi\epsilon_0}\frac{\pi e^2}{m_{\rm e}c} g f \frac{1}{\sqrt{\pi}\Delta\nu_{\rm D}} N_{\rm H} A_{\rm Fe} A_{24+} A_{1s},$$

$$\Delta\nu_{\rm D} \equiv \frac{E_0}{hc}\sqrt{\frac{2k_{\rm B}T}{m_{\rm Fe}}}$$

- Medium can be $\tau < 1$ for continuum & $\tau \gg 1$ for lines.

Optical thickness τ_ν

τ_ν changes drastically as ν.
Assume a typical photoionized plasma around AGNs and X-ray binaries.

- $N_{\rm H} = 10^{24}$ cm^{-2}.
- $\log \xi = 3$, where ionization par $\xi = \frac{L_X}{4\pi n_e r^2}$

↓

- For continuum (electron scattering), $\tau_{\rm es} = N_{\rm H}\sigma_{\rm Th} = 0.67$
- For line (e.g., Fe XXV Heα resonance), $\tau_{\rm Fe\ He\alpha,r} = 4.7 \times 10^3$

$$\tau_{\rm Fe\ He\alpha,r} = \frac{1}{4\pi\epsilon_0}\frac{\pi e^2}{m_{\rm e}c} g f \frac{1}{\sqrt{\pi}\Delta\nu_{\rm D}} N_{\rm H} A_{\rm Fe} A_{24+} A_{1s},$$

$$\Delta\nu_{\rm D} \equiv \frac{E_0}{hc}\sqrt{\frac{2k_{\rm B}T}{m_{\rm Fe}}}$$

- Medium can be $\tau < 1$ for continuum & $\tau \gg 1$ for lines.

Line profile for $\tau \gg 1$

Resonance "scattering": Absorption & immediate emission (large A).

- Line photons with $\tau \gg 1$ diffuse not in space but in wavelength (into damping wing of Voigt profile before escape w. one long flight).
- Analytical solution for plane-parallel (Harrington73[5], Neufeld91[10]) or spherical (Dijkstra+06[2]) medium, 1D, uniform n.
- Profile can be resolved with *Resolve*, but not with HETGS, RGS.

$$J(x) = \frac{\sqrt{\pi}}{\sqrt{24} a\tau_0} \frac{x^2}{1 + \cosh\left[\sqrt{\frac{2\pi^3}{27}\frac{|x^3|}{a\tau_0}}\right]}, x \equiv \frac{\nu - \nu_0}{\Delta\nu_D}$$

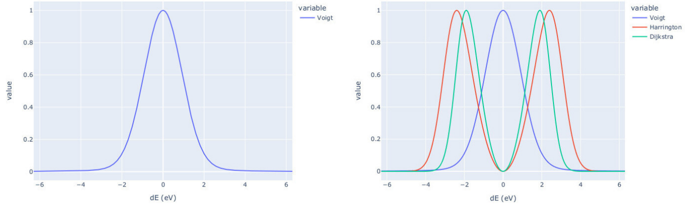

Figure 2. Normalized line profile for Fe XXVI Lyα ($N_H = 10^{23.5}$ cm^{-2}, T = 10 MK).

Numerical RT calculation

- RT calculation mandatory to interpret XRISM spectra.
- Numerical calculation need to implement:
  - All relevant γ-atom interactions ($\sigma_{\rm bb}(E)$, $\sigma_{\rm bf}(E)$, $\sigma_{\rm ff}(E)$).
  - All relevant atomic properties (A_{ij}, B_{ij}, C_{ij}, E_i, f_i, g_i).
  - Propagation of γ through medium with κ_ν, ϵ_ν, β_ν.
  - 3D profile of medium ($n(\vec{x})$, $T(\vec{x})$, $\vec{v}(\vec{x})$).
- Representative solvers and implementations.

Table 1. Representative solvers and implementations in numerical RT in X-rays.

Solver	Implementation
Accelerated Λ iteration	(LIME)
Discrete-ray	xstar [7], cloudy [1], spex (pion)
Monte Carlo	SKIRT [16], MONACO [17;12;11]

Numerical RT calculation

- RT calculation mandatory to interpret XRISM spectra.
- Numerical calculation need to implement:
  - All relevant γ-atom interactions ($\sigma_{\mathrm{bb}}(E)$, $\sigma_{\mathrm{bf}}(E)$, $\sigma_{\mathrm{ff}}(E)$).
  - All relevant atomic properties (A_{ij}, B_{ij}, C_{ij}, E_i, f_i, g_i).
  - Propagation of γ through medium with κ_ν, ϵ_ν, β_ν.
  - 3D profile of medium ($n(\vec{x})$, $T(\vec{x})$, $\vec{v}(\vec{x})$).
- Representative solvers and implementations.

Table 1. Representative solvers and implementations in numerical RT in X-rays.

Solver	Implementation
Accelerated Λ iteration	(LIME)
Discrete-ray	xstar[7], cloudy[1], spex (pion)
Monte Carlo	SKIRT[16], MONACO[17;12;11]

Numerical RT solvers/implementations

Table 2. Comparison between `xstar` versus `MONACO`

Solver	Two-stream	Monte Carlo
Implementation	`xstar`	`MONACO`
Dimension	1D	3D
$n(r)$ setup	yes	yes
$\vec{v}(r)$ setup	no	yes
Scattering	no	yes
γ-atom interaction	yes	partial[a]
Diffusion in λ	no[b]	yes
NLTE level & charge pop	yes	no
Thermal balance	yes	no
Momentum balance	no	no
Speed	fast	slow
Dynamic range	wide	narrow

[a] Only H- and He-like ions and neutral atoms supported.
[b] Escape probability is used.

Purpose of Study

We verify numerical RTs against observation data of a well-behaved source.

Outline

Super-Soft Source

- Observational features
  - Bright ($L_X \lesssim L_{Edd}$ of $1M_\odot$).
  - Very soft (peak at 20–100 eV).
  - $P_{orb} = 0.1 - 1$ day.
- Nature
  - Semi-detached binaries with accreting WD.
  - Steady burning on WD surface.

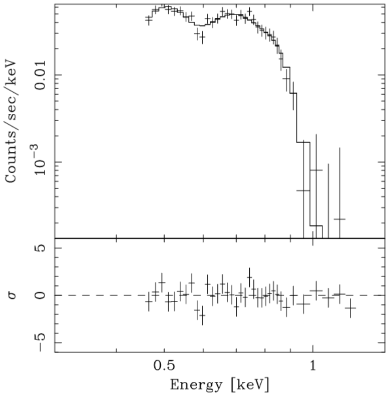

Figure 3. ASCA spectrum of CAL87 (Ebisawa+01 [4]).

CAL87

- SSS in LMC (Long+81[8]). $P_{\rm orb}$ = 10.6 hr (Pakull+88[13])
- ADC for shallow, long X-ray eclipse (Schmidtke+93[15], Ebisawa+01[4])

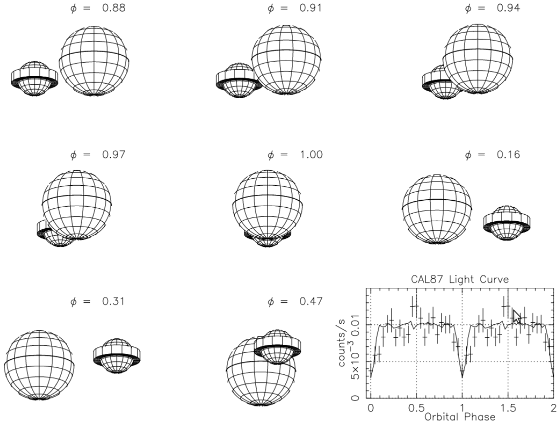

Figure 4. Simulation of X-ray light curve (Ebisawa+01[4])

Outline

Characterization of spectra (1) Continuum

Observations

- XMM-Newton EPIC (MOS, pn) for CCDs & RGS for grating.
- 2003/04/28 for 21.8 hours.

Phenomenological fitting using MOS spectra.

- $N_{\rm H}$ (LMC) × $N_{\rm H}$ (MW) × BB × edges (OVII K, OVIII K).

Table 3. Continuum model

Parameter		Value
Gal abs	$N_{\rm H}^{\rm Gal.}$ (10^{21} cm^{-2})	0.758 (fix)
LMC abs	$N_{\rm H}^{\rm LMC}$ (10^{21} cm^{-2})	3.61±0.02
Blackbody	$kT_{\rm BB}$ (eV)	$80.1^{+0.3}_{-0.2}$
	Norm. ($\times 10^{-4}$)	5.67 ± 0.06
Edge energy	$E_{\rm O\,VIII}$ (keV)	0.885±0.004
	$E_{\rm O\,VII}$ (keV)	0.743±0.002
Abs edge depth	$\tau_{\rm O\,VIII}$	$2.59^{+0.27}_{-0.13}$
	$\tau_{\rm O\,VII}$	$1.22^{+0.05}_{-0.11}$
Luminosity	$L_{\rm bol}$ (10^{37} erg s^{-1})	1.39 ± 0.17
$\chi^2_{\rm red}$ (dof)		1.20 (1744)

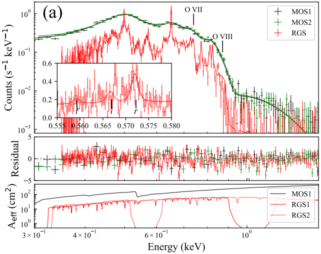

Figure 5. MOS and RGS spectra

Characterization of spectra (1) Continuum

Observations

- XMM-Newton EPIC (MOS, pn) for CCDs & RGS for grating.
- 2003/04/28 for 21.8 hours.

Phenomenological fitting using MOS spectra.

- N_{H} (LMC) × N_{H} (MW) × BB × edges (OVII K, OVIII K).

Table 3. Continuum model

Parameter		Value
Gal abs	$N_{\mathrm{H}}^{\mathrm{Gal.}}$ (10^{21} cm^{-2})	0.758 (fix)
LMC abs	$N_{\mathrm{H}}^{\mathrm{LMC}}$ (10^{21} cm^{-2})	3.61±0.02
Blackbody	kT_{BB} (eV)	$80.1^{+0.3}_{-0.2}$
	Norm. ($\times 10^{-4}$)	5.67 ± 0.06
Edge energy	$E_{\mathrm{O\,VIII}}$ (keV)	0.885±0.004
	$E_{\mathrm{O\,VII}}$ (keV)	0.743±0.002
Abs edge depth	$\tau_{\mathrm{O\,VIII}}$	$2.59^{+0.27}_{-0.13}$
	$\tau_{\mathrm{O\,VII}}$	$1.22^{+0.05}_{-0.11}$
Luminosity	L_{bol} (10^{37} erg s^{-1})	1.39 ± 0.17
χ^2_{red} (dof)		1.20 (1744)

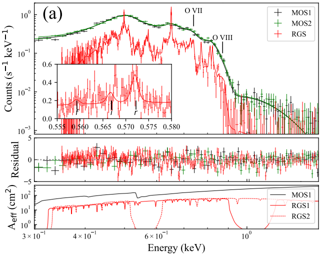

Figure 5. MOS and RGS spectra

Characterization of spectra (2) Lines

Phenomenological fitting using RGS spectra for 7 line complexes.

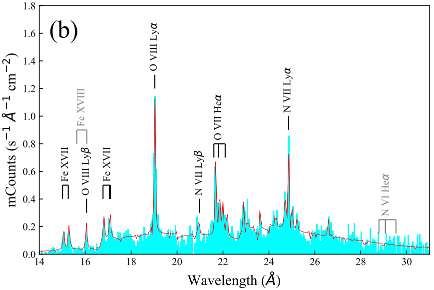

Figure 6. RGS spectra

Table 4. Fe XVII lines

	Upper level[a]	E (keV)	gf[b]	ϵ[c](cm^3 s^{-1})
3C	$(2s)^2(2p)^5(3d)^1\ ^1P_1$	0.826	2.49	1.8×10^{-15}
3D	$(2s)^2(2p)^5(3d)^1\ ^3D_1$	0.812	0.64	0.6×10^{-15}
3F	$(2s)^2(2p)^5(3s)^1\ ^3P_1$	0.738	0.10	1.1×10^{-15}
3G	$(2s)^2(2p)^5(3s)^1\ ^1P_1$	0.726	0.13	1.5×10^{-15}

[a] Lower level is the ground state $(2s)^2(2p)^6\ ^1S_0$ for all.
[b] Weighted oscillator strength.
[c] Emissivity for the collisionally ionized plasma at a temperature of 0.6 keV.

Figure 7. Line fitting results

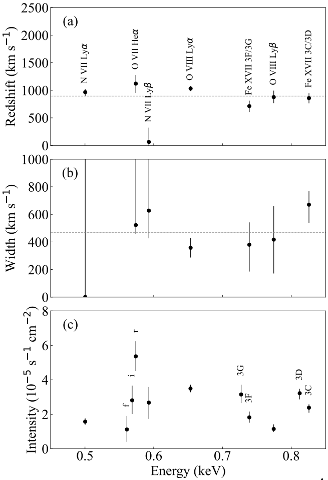

Constraint on $\xi \equiv \frac{L_X}{4\pi n r^2} \sim 10^{2.5}$

By presence (N VII, O VII/VIII, Fe XVII) & absence (N VI, Fe XVI/XVIII).

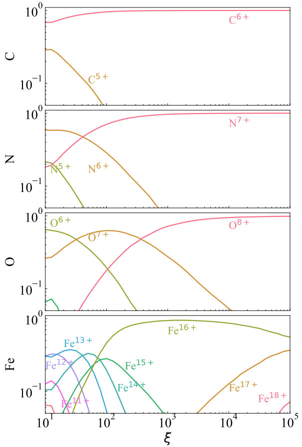

Figure 8. Charge population

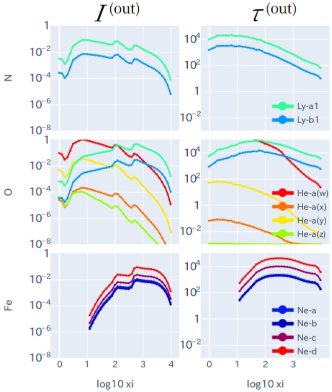

Figure 9. Line intensity and τ

Outline

Setup

1. Static.
2. Spherically symmetric.
3. Point-like WD at center.
4. Corona surrounds WD.
5. Incident completely blocked.
6. $v_{\rm bulk} = 0$.

* All constraints but 1 relaxed in Tominaga24 for Cir X-1.

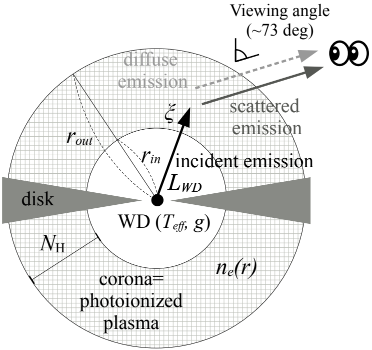

Parameters:

- Model: $r_{\rm in}$, $N_{\rm H}$, $n_{\rm e}(r)$, ξ, $L_{\rm WD}$, $M_{\rm WD}$, $g_{\rm WD}$, $T_{\rm eff}$.
- Obs: $r_{\rm out} = 4.8 \times 10^{10}$ cm, $i = 73$ deg (eclipse), $L_{\rm obs} = 1.4 \times 10^{37}$ erg s^{-1}.

Setup

1. Static.
2. Spherically symmetric.
3. Point-like WD at center.
4. Corona surrounds WD.
5. Incident completely blocked.
6. $v_{\mathrm{bulk}} = 0$.

* All constraints but 1 relaxed in Tominaga24 for Cir X-1.

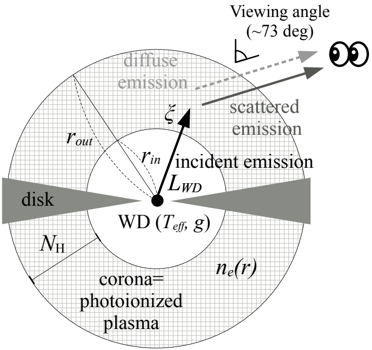

Parameters:

- Model: r_{in}, N_{H}, $n_{\mathrm{e}}(r)$, ξ, L_{WD}, M_{WD}, g_{WD}, T_{eff}.
- Obs: $r_{\mathrm{out}} = 4.8 \times 10^{10}$ cm, $i = 73$ deg (eclipse), $L_{\mathrm{obs}} = 1.4 \times 10^{37}$ erg s^{-1}.

Analytical estimation

$$L_{\rm obs} = (1 - e^{-\tau_{\rm es}})L_{\rm WD}$$
$$\tau_{\rm es} = \sigma_{\rm Th} N_{\rm e} = \sigma_{\rm Th} N_{\rm H}$$
$$n_{\rm e}(r) = n_{\rm e,in}\left(\frac{r}{r_{\rm in}}\right)^{-2}$$
$$N_{\rm e} = \int_{r_{\rm in}}^{r_{\rm out}} n_{\rm e}(r)dr$$
$$= n_{\rm e,in} r_{\rm in}^2 \left(\frac{1}{r_{\rm in}} - \frac{1}{r_{\rm out}}\right)$$
$$\xi = L_{\rm WD}/n_{\rm e,in} r_{\rm in}^2 \sim 10^{2.5}$$
$$L_{\rm WD} = 4\pi R_{\rm WD}^2 \sigma_{\rm SB} T_{\rm eff}^4$$
$$g = G M_{\rm WD}/R_{\rm WD}^2$$
$$R_{\rm WD} = 7.8\times10^8\ ({\rm cm}) \times \sqrt{\left(\frac{1.44 M_\odot}{M_{\rm WD}}\right)^{\frac{2}{3}} - \left(\frac{M_{\rm WD}}{1.44 M_\odot}\right)^{\frac{2}{3}}}$$

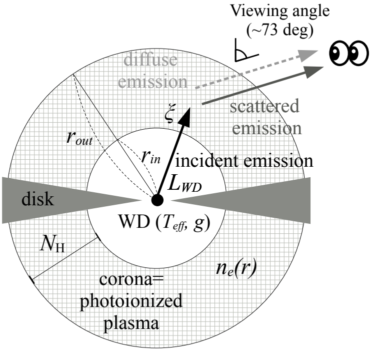

Analytical estimation

- Physical relations reduce the parameter to one $\alpha \equiv \frac{L_{\rm obs}}{L_{\rm WD}}$.
- $0 < \alpha \leq 1$, but has real solutions only in $0.2 < \alpha < 0.3$.
- All model parameters determined almost uniquely.

Good test bench to verify RT calc.

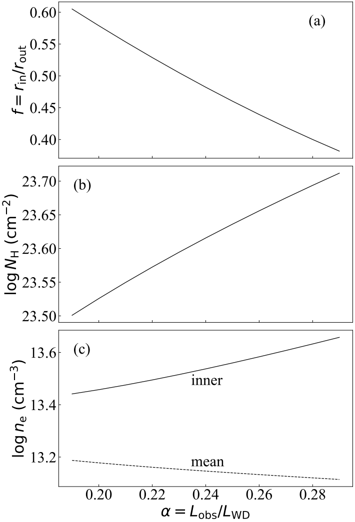

Analytical estimation

- Physical relations reduce the parameter to one $\alpha \equiv \frac{L_{\rm obs}}{L_{\rm WD}}$.
- $0 < \alpha \leq 1$, but has real solutions only in $0.2 < \alpha < 0.3$.
- All model parameters determined almost uniquely.

Good test bench to verify RT calc.

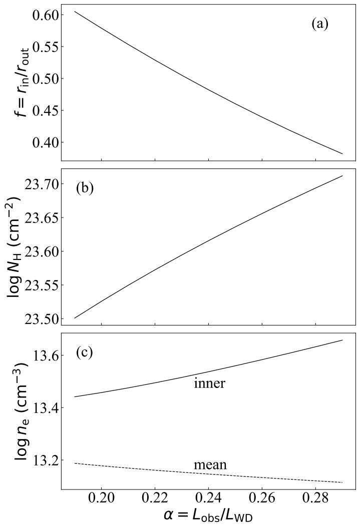

Numerical calculation (1) `xstar`

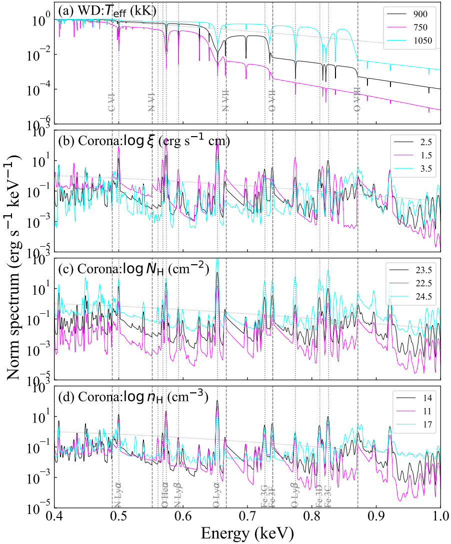

- `TMAP` WD atmosphere model (Rauch+10[14]) for incident spectrum.
- Parameters.
  - WD: $T_{\rm eff}$, $\log g = 9$.
  - Corona : ξ, $N_{\rm H}$, $\log n_{\rm e} = 14$.
- `xspec` table model made.
- Best-fit model.

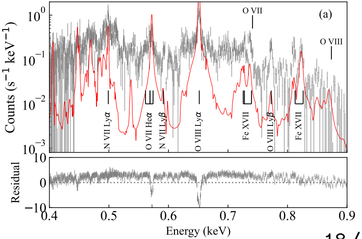

Numerical calculation (2) `MONACO`

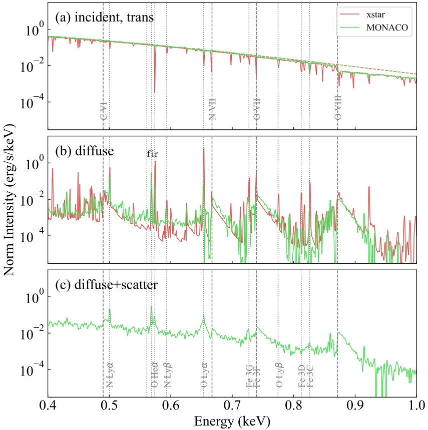

- 5×10^5 photons per grid of (ξ, N_H). JSS3 used.
- `TMAP` WD atmosphere model (Rauch+10[14]) for incident spectrum.
- `xspec` table model made.
- Best-fit model (diffuse+scatter).

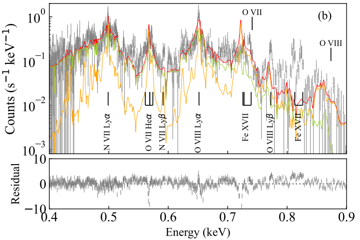

Comparison between models and data

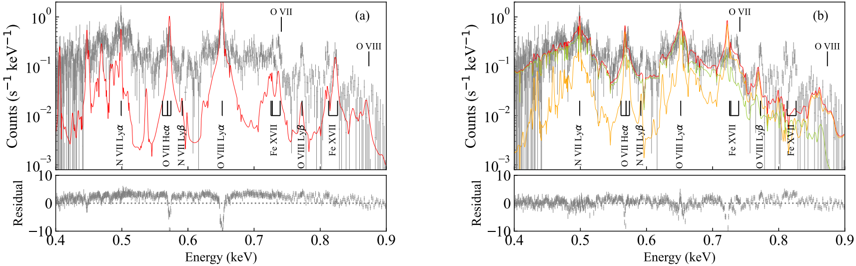

Four major discrepancies between RT codes and observation.

1. Continuum: `xstar` no way (no scattering). `MONACO` good.
2. Line intensity: `xstar` too strong (likely due to escape prob approx). `MONACO` too weak (likely due to lack of radiative excitation).
3. Line profile: `xstar` no way (all Voigt). `MONACO` makes attempts.
4. Line ratio:
   a. O VII Heα triplet : `xstar` good. `MONACO` bad (no NLTE level pop).
   b. O VIII Lyman decrement Lyβ/Lyα: `xstar` bad. `MONACO` bad.
   c. Fe XVII 3d→2p (3C,3D)/3s→2p (3F,3G): `xstar` bad. `MONACO` bad.

Comparison between models and data

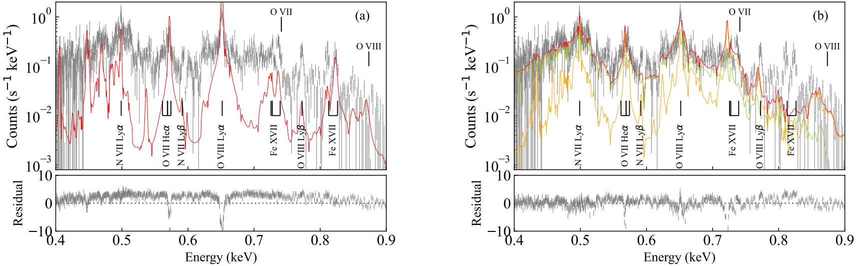

Four major discrepancies between RT codes and observation.

1. Continuum: `xstar` no way (no scattering). `MONACO` good.
2. Line intensity: `xstar` too strong (likely due to escape prob approx). `MONACO` too weak (likely due to lack of radiative excitation).
3. Line profile: `xstar` no way (all Voigt). `MONACO` makes attempts.
4. Line ratio:
   a. O VII Heα triplet : `xstar` good. `MONACO` bad (no NLTE level pop).
   b. O VIII Lyman decrement Lyβ/Lyα: `xstar` bad. `MONACO` bad.
   c. Fe XVII 3d→2p (3C,3D)/3s→2p (3F,3G): `xstar` bad. `MONACO` bad.

Outline

Conclusion

- X-ray line spectroscopy is prime focus of XRISM.
- RT undoubtedly needed.
- No code meets the data quality of current X-ray spectrometers.
  - Many discrepancies even for grating spectra of a well-behaved source.
  - More serious for μ-calorimeter spectra of non well-behaved sources
- What we should do next?
  - Develop RT codes focusing on X-ray line photon propagation.
  - Benchmark.
    - Among two-stream solvers (Lexington BM, Mehdipour+16 [9]).
    - Among Monte Carlo solvers (v/d Muelen+23 [16]).
    - Among diff solvers (Hubeney01 [6], Dumont03 [3]).
    - Against obs with lines & profiles (Tominaga24 for Cir X-1, MT+24 for CAL87).
  - Compromise with reality. Hybrid approach (mixture of diff solvers) useful if underlying assumptions properly understood.

Conclusion

- X-ray line spectroscopy is prime focus of XRISM.
- RT undoubtedly needed.
- No code meets the data quality of current X-ray spectrometers.
  - Many discrepancies even for grating spectra of a well-behaved source.
  - More serious for μ-calorimeter spectra of non well-behaved sources
- What we should do next?
  - Develop RT codes focusing on X-ray line photon propagation.
  - Benchmark.
    - Among two-stream solvers (Lexington BM, Mehdipour+16[9]).
    - Among Monte Carlo solvers (v/d Muelen+23[16]).
    - Among diff solvers (Hubeney01[6], Dumont03[3]).
    - Against obs with lines & profiles (Tominaga24 for Cir X-1, MT+24 for CAL87).
  - Compromise with reality. Hybrid approach (mixture of diff solvers) useful if underlying assumptions properly understood.

Conclusion

- X-ray line spectroscopy is prime focus of XRISM.
- RT undoubtedly needed.
- No code meets the data quality of current X-ray spectrometers.
  - Many discrepancies even for grating spectra of a well-behaved source.
  - More serious for μ-calorimeter spectra of non well-behaved sources
- What we should do next?
  - Develop RT codes focusing on X-ray line photon propagation.
  - Benchmark.
    - Among two-stream solvers (Lexington BM, Mehdipour+16 [9]).
    - Among Monte Carlo solvers (v/d Muelen+23 [16]).
    - Among diff solvers (Hubeney01 [6], Dumont03 [3]).
    - Against obs with lines & profiles (Tominaga24 for Cir X-1, MT+24 for CAL87).
  - Compromise with reality. Hybrid approach (mixture of diff solvers) useful if underlying assumptions properly understood.

Conclusion

- X-ray line spectroscopy is prime focus of XRISM.
- RT undoubtedly needed.
- No code meets the data quality of current X-ray spectrometers.
  - Many discrepancies even for grating spectra of a well-behaved source.
  - More serious for μ-calorimeter spectra of non well-behaved sources
- What we should do next?
  - Develop RT codes focusing on X-ray line photon propagation.
  - Benchmark.
    - Among two-stream solvers (Lexington BM, Mehdipour+16[9]).
    - Among Monte Carlo solvers (v/d Muelen+23[16]).
    - Among diff solvers (Hubeney01[6], Dumont03[3]).
    - Against obs with lines & profiles (Tominaga24 for Cir X-1, MT+24 for CAL87).
  - Compromise with reality. Hybrid approach (mixture of diff solvers) useful if underlying assumptions properly understood.

Conclusion

- X-ray line spectroscopy is prime focus of XRISM.
- RT undoubtedly needed.
- No code meets the data quality of current X-ray spectrometers.
  - Many discrepancies even for grating spectra of a well-behaved source.
  - More serious for μ-calorimeter spectra of non well-behaved sources
- What we should do next?
  - Develop RT codes focusing on X-ray line photon propagation.
  - Benchmark.
    - Among two-stream solvers (Lexington BM, Mehdipour+16[9]).
    - Among Monte Carlo solvers (v/d Muelen+23[16]).
    - Among diff solvers (Hubeney01[6], Dumont03[3]).
    - Against obs with lines & profiles (Tominaga24 for Cir X-1, MT+24 for CAL87).
  - Compromise with reality. Hybrid approach (mixture of diff solvers) useful if underlying assumptions properly understood.

Conclusion

- X-ray line spectroscopy is prime focus of XRISM.
- RT undoubtedly needed.
- No code meets the data quality of current X-ray spectrometers.
  - Many discrepancies even for grating spectra of a well-behaved source.
  - More serious for μ-calorimeter spectra of non well-behaved sources
- What we should do next?
  - Develop RT codes focusing on X-ray line photon propagation.
  - Benchmark.
    - Among two-stream solvers (Lexington BM, Mehdipour+16 [9]).
    - Among Monte Carlo solvers (v/d Muelen+23 [16]).
    - Among diff solvers (Hubeney01 [6], Dumont03 [3]).
    - Against obs with lines & profiles (Tominaga24 for Cir X-1, MT+24 for CAL87).
  - Compromise with reality. Hybrid approach (mixture of diff solvers) useful if underlying assumptions properly understood.

[1] P. Chakraborty, G. J. Ferland, M. Chatzikos, F. Guzmán, and Y. Su. X-Ray Spectroscopy in the Microcalorimeter Era. III. Line Formation under Case A, Case B, Case C, and Case D in H- and He-like Iron for a Photoionized Cloud. ApJ, 912(1):26, April 2021.

[2] Mark Dijkstra, Zoltán Haiman, and Marco Spaans. Lyα Radiation from Collapsing Protogalaxies. I. Characteristics of the Emergent Spectrum. ApJ, 649(1):14, September 2006.

[3] A.-M. Dumont, S. Collin, F. Paletou, S. Coupé, O. Godet, and D. Pelat. Escape probability methods versus "exact" transfer for modelling the X-ray spectrum of Active Galactic Nuclei and X-ray binaries. A&A, 407(1):13–30, August 2003.

[4] Ken Ebisawa, Koji Mukai, Taro Kotani, Kazumi Asai, Tadayasu Dotani, Fumiaki Nagase, H. W. Hartmann, J. Heise, P. Kahabka, and A. van Teeseling. X-Ray Energy Spectra of the Supersoft X-Ray Sources CAL 87 and RX J0925.7-4758 Observed with ASCA. ApJ, 550(2):1007–1022, 2001.

[5] J. Patrick Harrington. The scattering of resonance-line radiation in the limit of large optical depth. MNRAS, 162(1):43–52, May 1973.

[6] Ivan Hubeny. From escape probabilities to exact radiative transfer. In Gary Ferland and Daniel Wolf Savin, editors, Spectroscopic

Challenges of Photoionized Plasmas, volume 247 of Astronomical Society of the Pacific Conference Series, page 197, January 2001.

[7] T. R. Kallman, P. Palmeri, M. A. Bautista, C. Mendoza, and J. H. Krolik. Photoionization Modeling and the K Lines of Iron. ApJS, 155(2):675–701, 2004.

[8] K. S. Long, D. J. Helfand, and D. A. Grabelsky. A soft X-ray study of the Large Magellanic Cloud. ApJ, 248:925, 1981.

[9] M. Mehdipour, J. S. Kaastra, and T. Kallman. Systematic comparison of photoionised plasma codes with application to spectroscopic studies of AGN in X-rays. A&A, 596:A65, December 2016.

[10] David A. Neufeld. The Escape of Lyman-Alpha Radiation from a Multiphase Interstellar Medium. ApJ, 370:L85, April 1991.

[11] Hirokazu Odaka. Detailed Modeling and Observational Verification of X-ray Reprocessing Astrophysical Objects. PhD thesis, The University of Tokyo, 2012.

[12] Hirokazu Odaka, Felix Aharonian, Shin Watanabe, Yasuyuki Tanaka, Dmitry Khangulyan, and Tadayuki Takahashi. X-RAY DIAGNOSTICS OF GIANT MOLECULAR CLOUDS IN THE

GALACTIC CENTER REGION AND PAST ACTIVITY OF Sgr A\ast. ApJ, 740(2):103, October 2011.

[13] M. W. Pakull, K. Beuermann, M. van der Klis, and J. van Paradijs. LHG 87, a new low-mass eclipsing X-ray binary in the LMC. A&AL, 203:L27–L30, September 1988.

[14] Thomas Rauch, Ellen Ringat, and Klaus Werner. Spectral Analyses Of The Hottest White Dwarfs: Grids Of Spectral Energy Distributions For Extremely Hot, Compact Stars In The Framework Of The Virtual Observatory. Proceeding of the Physics of Accreting Compact Binaries, pages 1–6, 2010.

[15] P. C. Schmidtke, T. K. McGrath, A. P. Cowley, and L. M. Frattare. The X-ray eclipse of the LMC binary CAL 87. PASP, 105:863, 1993.

[16] Bert Vander Meulen, Peter Camps, Marko Stalevski, and Maarten Baes. X-ray radiative transfer in full 3D with SKIRT. A&A, 674:A123, June 2023.

[17] Shin Watanabe, Masao Sako, Manabu Ishida, Yoshitaka Ishisaki, Steven M. Kahn, Takayoshi Kohmura, Fumiaki Nagase, Frederik Paerels, and Tadayuki Takahashi. X-Ray Spectral Study of the Photoionized Stellar Wind in Vela X-1. ApJ, 651(1):421–437, November 2006.